Current Profile and Energy Control in DIII-D Plasmas Using Discrete-Time Variable-Structure Control

Menno Lauret, William Wehner, Eugenio Schuster, Christopher T. Holcomb, Timothy C. Luce, John R. Ferron, Michael L. Walker, David A. Humphreys, Benjamin G. Penaflor and Robert D. Johnson

***Abstract*— One of the most promising candidates to produce clean nuclear fusion energy is the tokamak, a device magnetically confining an extremely hot plasma (i.e. an ionized gas) where the fusion reactions take place. To produce nuclear fusion energy using tokamak devices, it is crucial that the poloidal magnetic flux (characterized by the so-called q profile) and the plasma internal energy are tightly controlled to avoid magnetohydrodynamic instabilities and to reach the high pressures and temperatures that are needed for high fusion-power density. Simultaneous control of the q profile and the internal energy is challenging for a number of reasons: the system is nonlinear, there are significant parameter uncertainties and large disturbances, the available number of actuators is small, and the actuation authority is limited from a control perspective. Therefore, a variable-structure controller is proposed in this work to tackle this plasma control problem since this type of controllers can typically diminish the impact of serious disturbances and nonlinearities while still leading to good performance. Simulations and recent experiments on the DIII-D tokamak in a challenging high-confinement (H-mode) plasma regime show that this control approach does indeed lead to good and repeatable control of the q profile and the internal energy.**

I. Introduction

Nuclear fusion is a candidate for clean energy production that does create neither long term radioactive waste nor green house gasses. Moreover, it is virtually independent of scarce natural resources. When ions are brought together close enough under high temperature and density conditions, they fuse and a significant amount of energy is released due to mass-energy conversion. Research on how to use this nuclear process as a viable energy source started in the 1940s and has mainly, but not exclusively, focussed on magnetic confinement. As the fuel gas (isotopes of hydrogen) is heated to fusion conditions, it ionizes and becomes what is known as a plasma. In a plasma, separated ions and electrons have electrical charge, conduct electricity, and follow magnetic field lines. The magnetic confinement approach to fusion exploits this property of the plasma and employs magnetic fields to confine it within a specific volume, preventing in this way the hot ($\approx 10^8$ degrees) plasma from entering in contact with the inner wall of the fusion reactor. In the 1950s, the tokamak emerged as one of the most promising candidates for successful magnetically-confined nuclear fusion.

This work was supported in part by the U.S. Department of Energy (DE-SC0010661, DE-FC02-04ER54698). M. Lauret, W. Wehner, and E. Schuster (schuster@lehigh.edu) are with the Department of Mechanical Engineering and Mechanics, Lehigh University, Bethlehem, PA 18015, USA. C. Holcomb, T.C. Luce, J.R. Ferron, M.L. Walker, D.A. Humphreys, B.G. Penaflor, and R.D. Johnson are with General Atomics, San Diego, CA 92121, USA.

In a tokamak [1], a plasma is confined in a toroidal vessel by helical magnetic field lines, which are characterized by their toroidal and poloidal components. Any point within the toroidal plasma is characterized by its poloidal magnetic flux, which is defined as $\Psi = \int_S \bar{B}_\theta \cdot d\bar{S}$, where $\bar{B}_\theta$ denotes the poloidal component of the magnetic field and S is the surface normal to the z axis bounded by a toroidal ring passing through the point of interest. Points of equal poloidal magnetic flux define nested magnetic-flux surfaces as shown in Fig. 1. The axisymmetry provided by the toroidal geometry together with the selection of a spatial coordinate ρ indexing the nested magnetic-flux surfaces reduces the three-dimensional problem to just one dimension. The shape of any variable on this spatial coordinate is referred to as profile.

To create conditions under which nuclear fusion is possible, the plasma needs to have very high temperature, density, and energy confinement time (i.e. the typical time scale in which the plasma loses its energy). However, increasing these plasma variables also increases detrimental phenomena such as neoclassical tearing modes (NTMs) and other instabilities in the magnetic field (commonly referred to as MHD activity[1]). These phenomena can not only limit the realizable temperature and pressure and locally change the magnetic field but also lead to disruption and termination of the plasma. It has been shown that the profile of the safety factor q, which is a measure of the pitch of the magnetic field lines, plays an important role in avoiding these phenomena and achieving both steady-state and high-performance plasma conditions. If q has the "right" profile, with high enough values at the magnetic axis ($\rho = 0$) and at the plasma boundary, then many undesirable instabilities and plasma-degrading phenomena can be avoided.

In day-to-day operation of tokamaks, the q profile is controlled in open-loop by designing feedforward trajectories for the available actuators, which include the total plasma current and non-inductive current drives such as neutral-beam injectors and electron-cyclotron launchers. However, this does not always lead to good results because the initial conditions for the q profile vary between discharges. Moreover, magnetic and kinetic disturbances perturb the plasma state evolution, resulting in q profiles that are not close enough to the desired one. To increase the repeatability of discharges and to gain robustness against disturbances, feedback control of the q profile arises as a necessity.

[1]The MHD (magnetohydrodynamic) equations are a combination of the Maxwell and Navier-Stokes equations and describe the coupled fluid (plasma) and electromagnetic field dynamics.

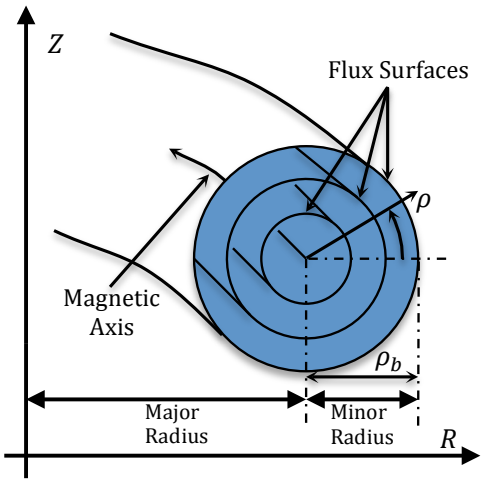

Fig. 1. The magnetic surfaces within a tokamak.

The kinetic-magnetic coupling and nonlinear infinite-dimensional nature of the problem has led to a model-based control approach based on both data-driven [2] and first-principles-driven [3], [4], [5], [6] modeling techniques. Model-based control methodologies that have been used in the last decade for q-profile regulation include LQR [7], MPC [8], Lyapunov-based control [9], backstepping control [10], and H_∞ control [11], [12]. Experiments typically shows that the q-profile feedback controller changes the internal energy of the plasma in an unwanted fashion while pursuing a desired profile. The change in energy (and temperature) varies the resistive diffusivity of the plasmas affecting the control performance, especially in the H-mode regime characterized by higher temperature and low resisitivity. More importantly, large changes in energy can also lead to serious MHD instabilities that must be avoided at all cost.

Therefore, closed-loop q-profile control in combination with internal-energy control is proposed in this work for the DIII-D tokamak in the form of a variable-structure controller. This type of controllers is robust against both model uncertainties and matched disturbances (i.e. disturbances that enter the state-space equations at the same place as an input) while it has the capability of achieving good performance. The idea behind variable-structure control is to steer the system state to a subspace, i.e. the sliding surface, by switching fast between two different high-gain control actions. Once the state is on this sliding surface, it converges exponentially to zero by design. It may be problematic for many actuators to achieve the desired fast switching required by variable-structure control. This is not the case, however, of the neutral beam powers in DIII-D, which are modulated between minimal and maximum power. Aggressive and saturated use of these actuators is therefore not a limitation and actually another reason for having designed this type of controller. The variable-structurel controller designed for q-profile regulation in DIII-D makes use of a discrete-in-time model, which leads to a discrete-time variable-structure controller (DVSC) that avoids some typical chattering issues and eases implementation. The sliding-mode controller proposed in [13] differs from our approach in several ways, which include the structure of the controller, the modeling of the kinetic-magnetic coupling through the plasma resistivity, the time domain representation, and experimental testing.

This article is organized as follows. The model for the q-profile and energy evolutions is introduced in Section II. In Section III the DVSC is constructed. The DIII-D experimental results presented in Section IV confirm that the approach works effectively in the difficult-to-control highly-disturbed H-mode plasma regime. Conclusions and suggestions for future work are stated in Section V.

II. Current Profile and Internal Energy model

A. Current Profile Model

The mean effective minor radius, ρ, is used to index each magnetic-flux surface in Fig. 1. It is related to the toroidal magnetic flux, Φ, and to the vacuum toroidal magnetic field at the geometric major radius R_0 of the tokamak, $B_{\phi,0}$, by means of $\pi B_{\phi,0}\rho^2 = \Phi$. The mean effective minor radius can be normalized as $\hat{\rho} = \rho/\rho_{\rm b}$, where $\rho_{\rm b}$ is the value of ρ at the last closed magnetic-flux surface. The safety factor $q(\hat{\rho},t)$ is defined in terms of the gradient of $\psi(\hat{\rho},t)$ as

$$q(\hat{\rho},t) = \frac{d\Phi}{d\Psi} = -\frac{d\Phi}{2\pi d\psi} = -\frac{B_{\phi,0}\rho_{\rm b}^2\hat{\rho}}{\partial\psi/\partial\hat{\rho}}, \qquad (1)$$

where t is the time and $\psi(\hat{\rho},t)$ is the poloidal stream function, which is closely related to the poloidal flux, i.e., $\Psi = 2\pi\psi$. Since the toroidal current density also depends on the gradient of $\psi(\hat{\rho},t)$, fusion plasma physicists speak interchangeably of the current (density) profile and the q profile. The evolution of the poloidal magnetic flux can be described by the magnetic diffusion equation [14],

$$\frac{\partial\psi}{\partial t} = \frac{\eta(T_{\rm e})}{\mu_0\rho_{\rm b}^2\hat{F}^2}\frac{1}{\hat{\rho}}\frac{\partial}{\partial\hat{\rho}}\left(\hat{\rho}\hat{F}\hat{G}\hat{H}\frac{\partial\psi}{\partial\hat{\rho}}\right) + R_0\hat{H}\eta(T_{\rm e})j_{\rm NI}, \quad (2)$$

where $\eta(T_{\rm e})$ is the plasma resistivity for which simplified scaling models are available [15] $T_{\rm e}(\hat{\rho},t)$ is the electron temperature, μ_0 is the vacuum permeability, $j_{\rm NI}(\hat{\rho},t)$ is the noninductive current density from various sources, $\hat{F}(\hat{\rho})$, $\hat{G}(\hat{\rho})$, and $\hat{H}(\hat{\rho})$ are spatially varying geometric factors pertaining to the magnetic configuration of a particular plasma equilibrium [3]. The boundary conditions are given by

$$\left.\frac{\partial\psi}{\partial\hat{\rho}}\right|_{\hat{\rho}=0} = 0, \quad \left.\frac{\partial\psi}{\partial\hat{\rho}}\right|_{\hat{\rho}=1} = -\frac{\mu_0}{2\pi}\frac{R_0}{\hat{G}|_{\hat{\rho}=1}\hat{H}|_{\hat{\rho}=1}}I_{\rm p}(t), \quad (3)$$

where $I_{\rm p}(t)$ is the total plasma current. Based on experimental observations at DIII-D, simplified scenario-oriented physics-based models for the plasma density, electron temperature, plasma resistivity, and noninductive current drives (including bootstrap current) in H-mode discharges were developed [6]. The model (2) can be written in the control-oriented form

$$\begin{aligned}\frac{\partial\psi}{\partial t}(\hat{\rho},t) &= \frac{f_\eta}{\hat{\rho}}\frac{\partial}{\partial\hat{\rho}}\left(\hat{\rho}D_\psi\frac{\partial\psi}{\partial\hat{\rho}}\right)u_\eta(t)\\ &+ \sum_{i=1}^{n_{\rm NBI}} f_{{\rm NBI},i}u_{{\rm NBI},i}(t) + f_{\rm BS}\left(\frac{\partial\psi}{\partial\hat{\rho}}\right)^{-1}u_{\rm BS}(t).\end{aligned} \qquad (4)$$

The term n_{NBI} denotes the number of neutral beam injectors, $D_\psi = \hat{F}\hat{G}\hat{H}$, the functions $f_{(\cdot)}(\hat{\rho})$ capture the spatial dependence of the model (the form of these functions arise from the physics-based correlations for density, temperature, resistivity, and auxiliary current drive [6]) and $u_{(\cdot)}(t)$ are a set of nonlinear input functions of the form,

$$\begin{aligned} u_\eta(t) &= I_{\text{p}}(t)^{-3/2} P_{\text{tot}}(t)^{-3/4} \bar{n}_{\text{e}}(t)^{3/2}, \\ u_{\text{NBI},i}(t) &= I_{\text{p}}(t)^{-1} P_{\text{tot}}(t)^{-1/2} P_{\text{NBI},i}(t), \\ u_{\text{BS}}(t) &= I_{\text{p}}(t)^{-1/2} P_{\text{tot}}(t)^{-1/4} \bar{n}_{\text{e}}(t)^{3/2}, \end{aligned} \tag{5}$$

where $P_{\text{tot}}(t)$ is the total power injected to the plasma, $P_{\text{NBI},i}(t)$ represents the individual neutral-beam injector powers, and $\bar{n}_{\text{e}}(t)$ is the line-averaged electron density. Electron-cyclotron launcher powers are not used for feedback control in this work and for this reason their effects are not included in the model. The system admit diffusivity control (u_η), interior control ($u_{\text{NBI},i}, u_{\text{BS}}$), and boundary control (I_{p}).

B. Internal Energy Model

The plasma internal energy, i.e. the volume averaged energy density over the plasma volume, can be written as

$$W = \int_{\hat{\rho}} \left(\frac{3}{2} n_e(\hat{\rho}, t) T_e(\hat{\rho}, t) + \frac{3}{2} n_i(\hat{\rho}, t) T_i(\hat{\rho}, t) \right) \frac{dV}{d\hat{\rho}} d\hat{\rho}. \tag{6}$$

Its dynamics can be well approximated by

$$\frac{dE}{dt} = -\frac{E}{\tau_{\text{E}}} + P_{\text{tot}}(t), \tag{7}$$

where τ_{E} is a the global energy confinement time. We use the ITER-98 (IPB98$(y, 2)$) [16] scaling law to model the energy confinement time, $\tau_E \propto I_p^{0.93} \bar{n}_e^{0.41} P_{tot}^{-0.69}$. The total absorbed power, P_{tot} is equal to the auxiliary power injected into the plasma by the neutral beams, $P_{\text{aux}} = \sum_i^{n_{\text{NBI}}} P_{\text{NBI},i}$, plus the power from the ohmic coil, P_{ohm}, minus the radiative power, P_{rad}, i.e. $P_{\text{tot}} = P_{\text{aux}} + P_{\text{ohm}} - P_{\text{rad}}$. The ohmic heating power can be computed as,

$$j_{\text{tor}} = -c_1 \frac{\partial}{\partial \hat{\rho}} \left(c_2 \frac{\partial \psi}{\partial \hat{\rho}} \right), P_{ohm} = \int_V j_{\text{tor}}(\hat{\rho}, t)^2 \eta(\hat{\rho}, t) dV, \tag{8}$$

where c_1 and c_2 are time-constant profiles [6]. The radiative power (Bremsstrahlung radiation) can be expressed as

$$P_{\text{rad}} = k_{\text{brem}} Z_{\text{eff}} n_e(\hat{\rho}, t)^2 \sqrt{T_e(\hat{\rho}, t)}, \tag{9}$$

where $k_{\text{brem}} = 5.5 \times 10^{-37}$ Wm$^3/\sqrt{keV}$ is the Bremsstrahlung radiation coefficient and Z_{eff} is the effective ion atomic number [17].

C. Discretized Model

The models for $\psi(\hat{\rho}, t)$ (2)–(3) and $W(t)$ (7) evolutions are spatially and temporally discretized with a time step $\Delta t = 0.020$ s and a spatial step $\Delta\hat{\rho} = 0.05$. Then, the dynamics is written in terms of the rotational transform $\iota = 1/q = -(\partial\psi/\partial\hat{\rho})/B_{\phi,0}\rho_b^2\rho$. This results in a state $x(k) = [\iota(\hat{\rho} = 0.05, k), \iota(\hat{\rho} = 0.1, k), \ldots, \iota(\hat{\rho} = 0.95, k), W(k)]$ of size $n = 20$, with $k \in \mathbb{N}$. After linearizing the equations for ι and W around a nominal trajectory, the linearized discrete-time dynamics of the state is given by

$$x(k+1) = A(k)x(k) + Bu(k), \tag{10}$$

with $A \in \mathbb{R}^{n \times n}$, and $B \in \mathbb{R}^{n \times m}$, and input vector $u \in \mathbb{R}^m$.

III. Variable Strucutre Control

For reaching specific energy values and safety-factor profiles in a repeatable fashion in experiments, a control law has been designed to track a given reference $x_d(k)$ and thereby to control both $q(\hat{\rho}, t)$ and $W(t)$. The control law minimizes the tracking error $\tilde{x}(k) = x_d(k) - x(k)$ and thereby drives the plasma state to the desired q profile and W value. This state feedback controller uses all $n = 20$ measured states and m control inputs to the system. In this case $m = 5$ and the inputs are the plasma current I_p and four neutral beam powers. The discrete-time variable-structure controller is based on the discretized and linearized model (10). The specific control structure is based on [18] and has the form

$$u(k) = u_{ff}(k) + u_{lfb}(k) + u_{sfb}(k). \tag{11}$$

The feedforward input $u_{ff}(k)$ is either designed according to [19] or extracted from previous experiments. The two feedback components are a linear state feedback control

$$u_{lfb}(k) = \Gamma^{-1} M(x_d(k) - x(k)), \tag{12}$$

and nonlinear variable-structure control

$$u_{sfb}(k) = \Gamma^{-1} K \text{sat}(s(k), \phi), \tag{13}$$

with $s = G\tilde{x}$ is a sliding scalar variable and ϕ is a design constant scalar. The function sat$(s(k), \phi)$ is defined as

$$\text{sat}\,(s, \phi) = \begin{cases} \text{sign}(s), & |s| > \phi, \\ s/\phi, & |s| \leq \phi. \end{cases} \tag{14}$$

The matrices Γ, M, and $K = [K_1, K_2, \ldots, K_5]$ define the control law. To construct this controller for the given discrete-time linear system (10), first a linear state feedback matrix F is designed such that $A - BF$ has distinct and stable eigenvalues ($|\lambda_i| < 1$ for $i = 1, 2, \ldots, n$, as this is a discrete-time system). At least one eigenvalue is chosen to be real and in the $(-1, 1)$ interval. The matrix F can be designed using any suitable method, but in this work F has been designed by solving a discrete-time LQR problem that minimizes the quadratic cost function

$$J(u) = \sum_{n=1}^{\infty} (x(n)^T Q x(n) + u(n)^T R u(n)), \tag{15}$$

where Q and R are $n \times n$ and $m \times m$ weight matrices, respectively. One of the strictly-real stable eigenvalues of $A - BF$ is denoted as λ and the sliding variable s is defined as $s = G\tilde{x}$ with $G = \xi^T$, where ξ is the left eigenvector of $A - BF$ corresponding to the chosen eigenvalue λ. The matrix Γ can then be constructed as

$$\Gamma = \text{diag}(GB_1, \ldots, GB_5), \tag{16}$$

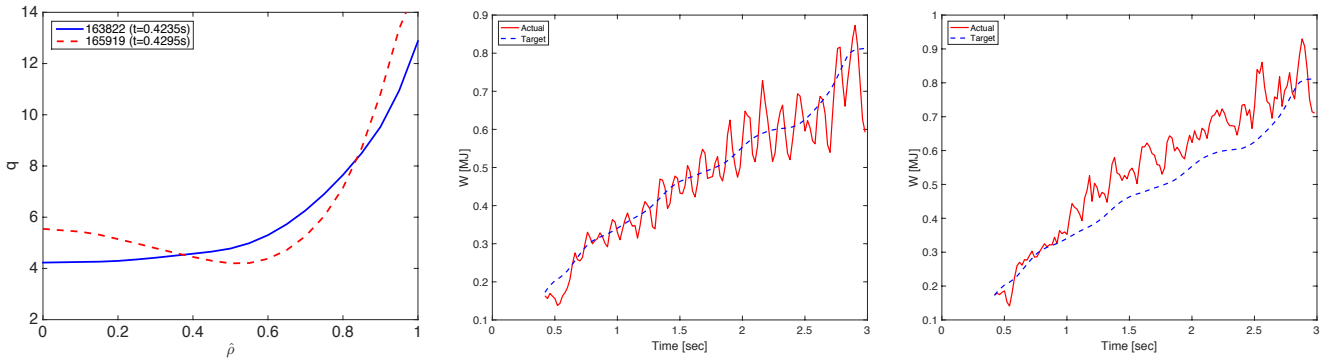

Fig. 2. Left: Although supposed to be similar discharges by design, the initial q profiles of discharge 165919 (red) and reference discharge 163822 (blue) are significantly different. Center: The internal energy $W(t)$ (red) follows the reference (blue) in discharge 165918. Right: The internal energy $W(t)$ (red) also follows the reference (blue) in discharge 165919 but with an offset. The energy typically oscillates in all discharges due to the sliding mode action.

where B_i is the i-th column of matrix B. The central idea of this variable-structure control approach is first to make the state converge towards $s = 0$, the stable sliding surface. Once the state resides on the $s = 0$ subspace, it will converge towards the origin as the reduced dynamics on the sliding surface is asymptoticaly stable by design and depends on the choice of λ. The saturation function $\text{sat}(s, \phi)$ in the feedback term u_{sfb} forces the state to converge to $s = 0$ and then keeps the state on the sliding surface, or at least in a boundary layer around it. The size of this boundary layer depends on the expected disturbances and is defined by the scalar ϕ. The definition of the saturation function in (14) shows how the, otherwise constant, control action u_{sfb} decreases in the boundary layer. The sliding gains $K_1, \ldots, K_5$ are designed such that the summation of the gains is high enough to overcome the disturbances and reach the boundary layer around the sliding surface [18]. As the disturbances in the real system are usually not well-known, these gains usually have to be chosen conservatively and adapted after experimental testing. Once all these scalars and matrices are defined, the matrix M can be computed as

$$M = \Gamma F - \phi^{-1} KG, \tag{17}$$

and the feedback control components u_{lfb} (12) and u_{sfb} (13) are fully determined.

IV. Experimental Setup and Results

A. Overall Objective

The goal of the experiment on DIII-D was to repeatedly and reliably track a desired q profile denoted by $q(\hat{\rho}, t)_{ref}$ and internal-energy value denoted by $W(t)_{ref}$ during the ramp-up and early flattop phases of the discharge ($t \in [0.4, 3]$ s) for arbitrary initial conditions (at $t = 0.4$ s) and unpredictable disturbances. These references (or targets) were slightly modified versions of the q profile and W value achieved in discharge 163822. This previously performed reference discharge is characterized by a monotonic q profile with a relatively high q_{min} of around 1.6 at $t = 3$ s, which favors plasma stability and performance. To keep the plasma in H-mode, a plasma regime with a temperature profile characterized by a high center value and a steep temperature gradient at the edge, it is necessary to sustain a minimal amount of auxiliary power during this discharge. To achieve this objective during the DIII-D experiment a lower bound ($3.5\ MW$) was imposed to the total NBI power and in this way transitions to low-confinement (L-mode) plasmas were avoided. After $t = 3$ s q-profile control was not longer pursued and the additional NBI power that became available from the two diagnostics beams was used to increase the energy W while sustaining the q profile achieved at $t = 3$ s by reducing the plasma resistivity (the q-profile dynamics becomes stiffer as $\eta \to 0$ as shown in (2)).

B. Summary of Experimental Results

The DVSC was tested in several discharges on the DIII-D tokamak with similar positive results. In many of the discharges some NBIs failed to work but the feedback controller was able to overcome these deficits and to achieve the target profile with the available actuation. We present experimental results from discharges 165918 and 165919 in this section. It is possible to note from Fig. 2 (left) that the initial condition for discharge 165919 was significantly different from the initial condition for the reference discharge 163822. This indeed was the case for all discharges. The shape of the initial q profile did impact the results of the experiment as it will be explained below because in general the controller could not match the reference profile until the end of the q-profile control phase ($\sim$ 3 s), when the perturbation in the initial condition was almost completely dissipated. However, and more importantly, the controller was always very successful in minimizing the matching error between actual and target q profiles in a least square sense at all times.

Fig. 2 also compares actual and reference internal-energy evolutions. Typically, the energy W is tracked relatively well in an average sense, but the energy is always oscillating due to the typical variable-structure switching action. In most of the discharges an offset is observed between actual and target energy values as shown in Fig. 2 (right) for shot 165919. In all these cases the actual energy is higher than the reference energy. This is probably due to the lower bound imposed on the NBI total power to avoid H-L transitions. Discharge 165918 was the only discharge in the experiment without this lower bound and the offset was not observed as shown in Fig. 2 (center). The energy oscillations due to the variable-

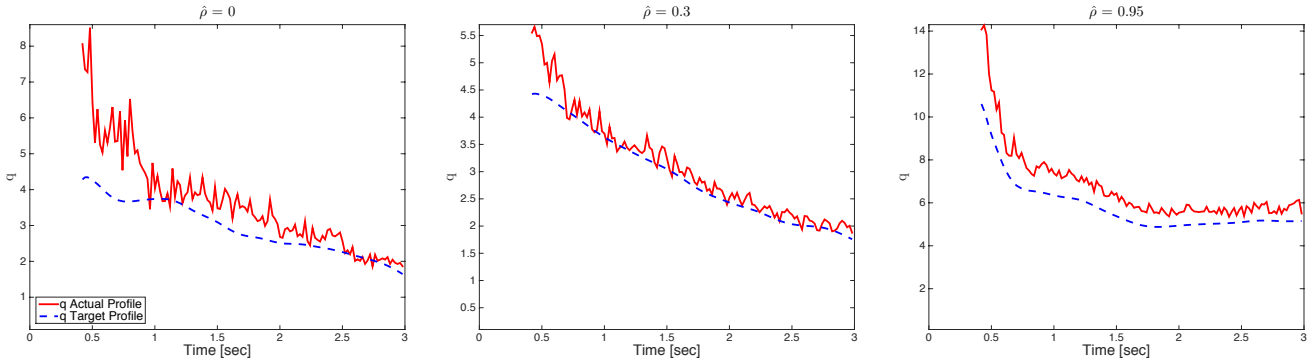

Fig. 3. Time evolution of $q(\hat{\rho}, t)$ (red) compared to the reference q-profile evolution (blue) shows relatively good tracking for shot 165918.

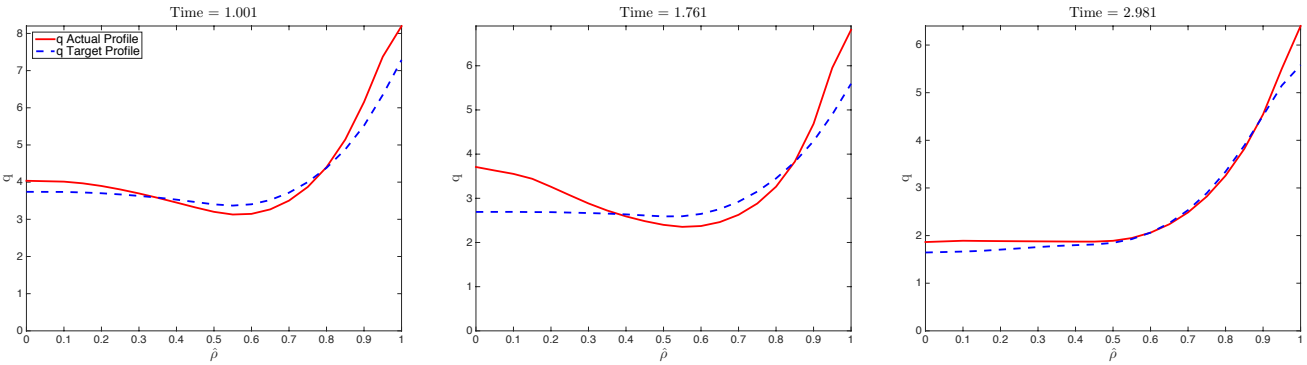

Fig. 4. Actual q profile (red) compared to reference q profile (blue) at several times. The controller tries to minimize the least square error between actual and target q profiles in shot 165918.

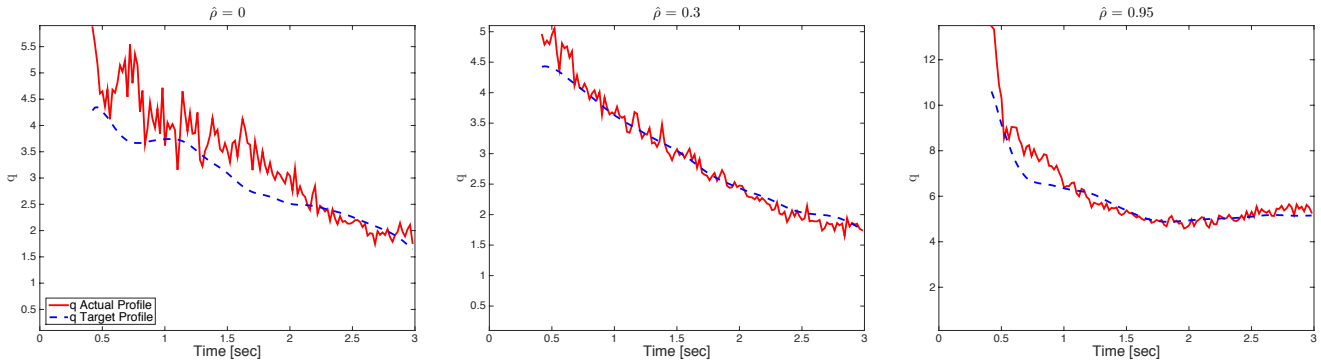

Fig. 5. Time evolution of $q(\hat{\rho}, t)$ (red) compared to the reference q-profile evolution (blue) shows relatively good tracking for shot 165919. Tracking is improved at the plasma edge.

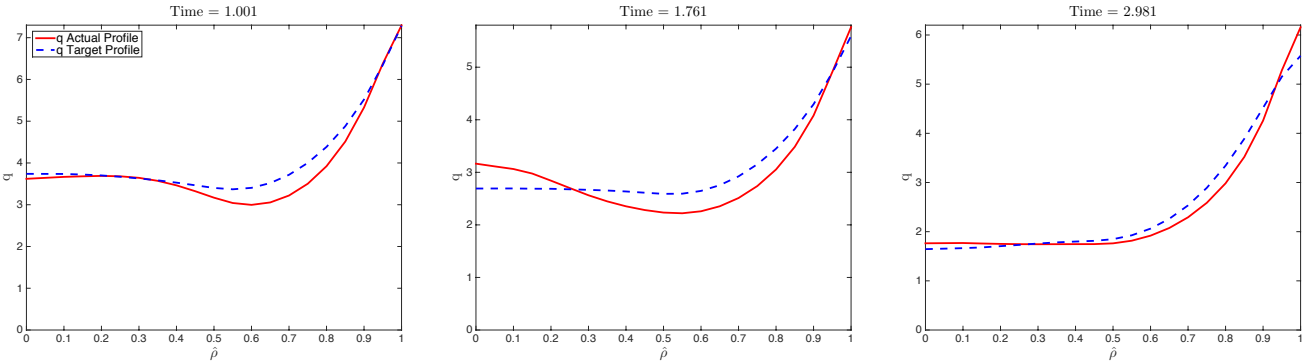

Fig. 6. Actual q profile (red) compared to reference q profile (blue) at several times. The controller tries to minimize the least square error between actual and target q profiles in shot 165919.

structurel control action did not introduce any problem in these discharges. However, tighter energy regulation with smaller oscillation levels (achievable with a different choice of control parameters) may be necessary in cases where the reference value gets close to stability limits.

Fig. 3 and Fig. 5 compare the time evolutions of both actual and target q profiles at $\hat{\rho} = 0, 0.3, 0.95$ for shots 165918 and 165919, respectively. Fig. 4 and Fig. 6 compare actual and target q profiles at $t = 1, 1.76, 2.98$ s also for shots 165918 and 165919, respectively. The tracking in the inner region ($\hat{\rho} = 0$) was challenged by both the difficulty to reconstruct the q profile evolution at the magnetic axis (note the noise level) and the perturbation in the initial condition. The tracking error decreased as initial perturbations faded away an the shapes of actual and target q profiles became similar. The tracking at $\hat{\rho} \approx 0.3$ was in general excellent because as shown by the snapshots in Fig. 4 and Fig. 6 this was the region where actual and target profiles met as the feedback controller tried to minimize the matching error in a least square sense. The tracking was not that excellent in the region defined by $0.3 < \hat{\rho} < 0.95$ due to once again the big perturbation in the initial conditions on the day of the experiment. As in the inner region, the tracking improved as the initial-condition perturbation faded away by the end of the q profile control phase. The tracking in the outer region ($\hat{\rho} = 0.95$) was in general very good due to effective plasma current regulation. When comparing Fig. 3 and Fig. 5 at $\hat{\rho} = 0.95$ it is possible to observe an improvement in tracking from shot 165918 to shot 165919. This behavior responds to two reasons. First, the variable-structure gain associated to the plasma current regulation was increased from shot 165918 to shot 165919. Second, and probably more importantly, a lower bound was imposed on the total beam power starting from shot 165919. The lower bound on the total beam power moved some of the priority originally put on energy regulation during the control synthesis to q-profile regulation since more beam power became available for q profile control at the expense of a larger tracking error for the internal energy as shown in Fig. 2. The later reason explains why the tracking error for the q profile was also reduced for $\hat{\rho} < 0.95$. As more beam power became available for q profile control, the controller could inject more non-inductive current through the beams and lower the q profile.

V. Summary and Conclusions

A discrete-time variable-structure controller for regulation of the plasma internal energy and safety factor profile of a tokamak plasma has been designed and tested experimentally on the DIII-D tokamak. The controller has been constructed using a discretized and linearized version of the underlying first-principles-driven model. The reason for using variable-structure control has been twofold. First, variable-structure control is robust against uncertainties and disturbances occurring in a tokamak plasma. Second, variable-structure control allows for very aggressive use of the control inputs, which is particularly well-suited for neutral beam injection. The controller has been tested in nonlinear transport simulations before experimental testing. The availability of the control-oriented transport model has been exploited to adjust the control-design parameters. Recent experiments on DIII-D show that the proposed control law indeed leads to successful tracking of the desired q profile and W value. This suggests that the inherent robustness of the variable-structure controller may indeed be beneficial for profile control under the highly disturbed conditions arising in H-mode plasmas in tokamaks. Use of electron-cyclotron heating and current drive for feedback control in future work has the potential to reduce energy oscillations and improve tracking performance.

References

[1] A. Pironti and M. Walker, "Fusion, tokamaks, and plasma control: an introduction and tutorial," *IEEE Control Systems Magazine*, vol. 25, no. 5, pp. 30–43, 2005.

[2] D. Moreau *et al.*, "Plasma models for real-time control of advanced tokamak scenarios," *Nuclear Fusion*, vol. 51, no. 063009, 2011.

[3] Y. Ou, T. Luce, E. Schuster *et al.*, "Towards model-based current profile control at DIII-D," *Fusion Engineering and Design*, vol. 82, pp. 1153–1160, 2007.

[4] E. Witrant *et al.*, "A control-oriented model of the current profile in tokamak plasmas," *Plasma Physics and Controlled Fusion*, vol. 49, pp. 1075–1105, 2007.

[5] F. Felici *et al.*, "Real-time physics-model-based simulation of the current density profile in tokamak plasmas," *Nuclear Fusion*, vol. 51, no. 083052, 2011.

[6] J. Barton, W. Shi *et al.*, "Physics-based control-oriented modeling of the safety factor profile dynamics in high performance tokamak plasmas," *52nd IEEE Conference on Decision and Control*, 2013.

[7] M. D. Boyer, J. Barton, E. Schuster *et al.*, "First-principles-driven model-based current profile control for the DIII-D tokamak via LQI optimal control," *Plasma Physics and Controlled Fusion*, vol. 55, no. 10, p. 105007, 2013.

[8] Y. Ou, E. Schuster, T. C. Luce, J. R. Ferron, M. L. Walker, and D. A. Humphreys, "Receding-Horizon Optimal Control of the Current Profile Evolution During the Ramp-up Phase of a Tokamak Discharge," *Control Engineering Practice*, vol. 19, pp. 22–31, 2011.

[9] F. B. Argomedo, E. Witrant, C. Prieur *et al.*, "Lyapunov-based distributed control of the safety-factor profile in a tokamak plasma," *Nuclear Fusion*, vol. 53, no. 3, p. 033005, 2013.

[10] M. D. Boyer, J. Barton, E. Schuster *et al.*, "Backstepping control of the toroidal plasma current profile in the DIII-D tokamak," *IEEE Trans. Control Systems Technology*, vol. 22, no. 5, pp. 1725–1739, Sept 2014.

[11] J. Barton, D. Boyer, W. Shi, E. Schuster *et al.*, "Toroidal current profile control during low confinement mode plasma discharges," *Nuclear Fusion*, vol. 52, no. 123018, 2012.

[12] J. Barton, K. Besseghir, J. Lister, and E. Schuster, "Physics-based control-oriented modeling and robust feedback control of the plasma safety factor profile and stored energy dynamics in ITER," *Plasma Physics and Controlled Fusion*, 2015.

[13] O. Gaye, E. Moulay, S. Brémond, L. Autrique, R. Nouailletas, J. Artaud, and Y. Orlov, "Robust stabilization of the current profile in tokamak plasmas using sliding mode approach in infinite dimension," *Control Engineering Practice*, vol. 21, p. 1350, 2013.

[14] F. Hinton and R. Hazeltine, "Theory of plasma transport in toroidal confinement systems," *Rev. Mod. Phys.*, vol. 48, pp. 239–308, 1976.

[15] O. Sauter *et al.*, "Neoclassical conductivity and bootstrap current formulas for general axisymmetric equilibria and arbitrary collisionality regime," *Physics of Plasmas*, vol. 6, no. 7, p. 2834, 1999.

[16] J. Snipes *et al.*, "Latest results on the H-mode threshold using the international H-mode threshold database," *Plasma Physics and Controlled Fusion*, vol. 42, 2000.

[17] J. Wesson, *Tokamaks*. Oxford, UK: Clarendon Press, 1984.

[18] C. Tang and E. Misawa, "Discrete variable structure control for linear multivariable systems," *J. Dyn. Syst. Meas. Control*, vol. 122, p. 783, 2000.

[19] J. Barton, E. Schuster *et al.*, "Nonlinear Physics-model-based Actuator Trajectory Optimization for Advanced Scenario Planning in the DIII-D Tokamak," in *19th IFAC World Congress*, 2014, pp. 671–676.